NANO LETTERS

2007
Vol. 7, No. 11
3452−3461

Nonfunctionalized Nanocrystals Can Exploit a Cell's Active Transport Machinery Delivering Them to Specific Nuclear and Cytoplasmic Compartments

Igor Nabiev,*,† Siobhan Mitchell,‡ Anthony Davies,‡ Yvonne Williams,‡ Dermot Kelleher,‡ Richard Moore,‡ Yurii K. Gun'ko,‡ Stephen Byrne,‡ Yury P. Rakovich,‡ John F. Donegan,‡ Alyona Sukhanova,† Jennifer Conroy,‡ David Cottell,§ Nikolai Gaponik,|| Andrey Rogach,⊥ and Yuri Volkov*,‡

EA No. 3798 Détection et Approches Thérapeutiques Nanotechnologiques dans les Mécanismes Biologiques de Défense, Université de Reims Champagne-Ardenne, 51100 Reims, France, CRANN Research Centre, Trinity College Dublin, Dublin 2, Ireland, University College Dublin, Dublin 4, Ireland, Physical Chemistry/Electrochemistry, Technische Universität Dresden, 01069 Dresden, Germany, and Department of Physics and Center for NanoScience (CeNS), Ludwig-Maximilians-Universität München, 80539 München, Germany

Received August 9, 2007; Revised Manuscript Received September 20, 2007

ABSTRACT

We use high content cell analysis, live cell fluorescent imaging, and transmission electron microscopy approaches combined with inhibitors of cellular transport and nuclear import to conduct a systematic study of the mechanism of interaction of nonfunctionalized quantum dots (QDs) with live human blood monocyte-derived primary macrophages and cell lines of phagocytic, epithelial, and endothelial nature. Live human macrophages are shown to be able to rapidly uptake and accumulate QDs in distinct cellular compartment specifically to QDs size and charge. We show that the smallest QDs specifically target histones in cell nuclei and nucleoli by a multistep process involving endocytosis, active cytoplasmic transport, and entering the nucleus via nuclear pore complexes. Treatment of the cells with an anti-microtubule agent nocodazole precludes QDs cytoplasmic transport whereas a nuclear import inhibitor thapsigargin blocks QD import into the nucleus. These results demonstrate that the nonfunctionalized QDs exploit the cell's active transport machineries for delivery to specific intranuclear destinations.

Currently well-established procedures yield a variety of colloidal quantum dots (QDs) with different functionalization, encoding their predictable cellular localization or molecular targets (NLS, antibody conjugates, etc.).[1−6] Paradoxically, the mechanisms of interaction of human cells with nonfunctionalized (i.e., not bearing specific functional localization sequence) QDs routinely manufactured in a number of laboratories worldwide have received far less attention. Although the evidence exist that the nontargeted negatively[7] and positively[8,9] charged QDs can be endocytosed by the human cells and even penetrate the cell nucleus,[10] almost all of these and many other studies[11−14] have been mainly focused on QDs toxicity effects whereas the intriguing mechanisms of QD interaction with cells remain to be defined. The lack of a lucid overall picture in this area could be explained by the limitations imposed by commonly used single cell microscopy analysis assays, precluding quantitative characterization of diverse or below average cell responses at the population level, contributed by cell cycle, cell type, and activation-associated phenomena. Here, we use high content cell analysis, live cell fluorescent imaging, and transmission electron microscopy (TEM) approaches combined with inhibitors of cellular transport and nuclear import to conduct the first systematic study of the mechanism of interaction of nonfunctionalized CdTe and CdSe/ZnS QDs with a panel of live human cells of different origin (macrophages, vascular endothelium, upper and lower gastrointestinal epithelium). We have based our choice of the cell types on the probability of the most common particle exposure sites in live organisms, involving phagocytic systems of the lung, skin, and mucosal surfaces, alimentary tract, and parenteral (via bloodstream) delivery routes. Live human

* Corresponding authors: yvolkov@tcd.ie (Y.V.); igor.nabiev@univ-reims.fr (I.N.).
† Université de Reims Champagne-Ardenne.
‡ Trinity College Dublin and CRANN Research Centre.
§ University College Dublin.
|| TU Dresden.
⊥ Ludwig-Maximilians-Universität.

10.1021/nl0719832 CCC: $37.00
Published on Web 10/19/2007

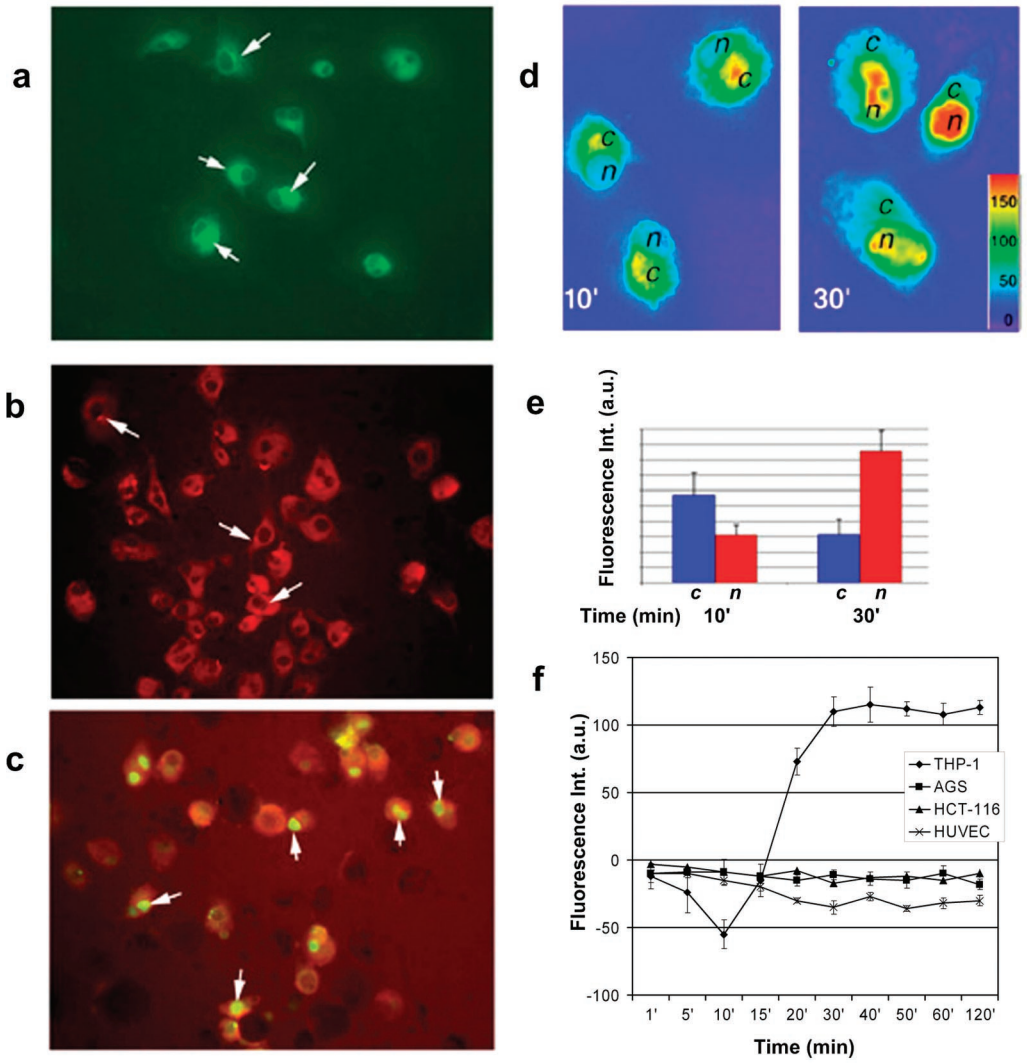

Figure 1. Intracellular localization of green (2.1 nm) and red (3.4 nm) CdTe QDs in the macrophage-like THP-1 cell line and epithelial cells. (a) Early stage green CdTe QD accumulation in THP-1 cells. THP-1 cells were incubated with green CdTe QDs (10 min). Arrows highlight early compact perinuclear localization. (b) Red CdTe QDs exhibit a cytoplasmic compartmentalization in the THP-1 cell line. THP-1 cells were incubated with red CdTe QDs for 30 min. Arrows highlight compact perinuclear localization. (c) Nuclear localization of green CdTe QDs in THP-1 cells. THP-1 cells were incubated with green and red CdTe QDs for 30 min. Arrows indicate complete green QD translocation to the nucleus (see also Supporting Information, Movie 1). (d) Analysis of green CdTe QDs intracellular distribution dynamics in individual cells. Pseudocolored images reflect integrated fluorescence intensity levels over the cytoplasmic and nuclear compartments. Left and right panels represent 10 and 30 min postincubation, respectively. Here "c" represents cytoplasm and "n" nucleus. Calibration bar indicates corresponding fluorescence intensity levels. Cell images are representative of more than five independent experiments. (e) Quantitative assessment of green CdTe QD uptake into the nucleus. Relative fluorescence units (RFU) convey the shift in green fluorescence from the cytoplasm c to the nucleus n over time. Mean values and standard errors calculated in 30 cells from randomly selected microscopic fields. (f) Quantitative dynamics of assessment of green CdTe QD uptake into the nucleus in cell lines indicated in the legend. *X* axis, time points (min); *Y* axis, difference in fluorescence intensity values registered in nuclear vs cytosolic compartments. Mean values and standard errors calculated for >300−400 cells from automatically collected microscopic fields.

macrophages are shown to be able to rapidly uptake and accumulate QDs in distinct cellular compartment specifically to QDs size and charge. We show that the smallest (2−3 nm in diameter) QDs specifically target histones in cell nuclei and nucleoli by a multistep process involving endocytosis, active cytoplasmic transport, and enter the nucleus via nuclear pore complexes (NPCs). Treatment of the cells with an anti-microtubule agent nocodazole precludes QDs cytoplasmic transport whereas a nuclear import inhibitor thapsigargin blocks QD import into the nucleus, but had no effect on QDs targeting to NPCs. These results clearly demonstrate that QDs exploit a cell's active transport machinery for delivery to discrete intracellular and intranuclear destinations.

Dynamics of QDs Nuclear Penetration. We initially incubated a panel of human cells of different lineages, incorporating primary monocyte-derived macrophages, macrophage-like cell line THP-1, vascular endothelial cells HUVEC, epithelial carcinoma cell lines AGS and HCT-116 (gastric and colonic origin, respectively) with the green-emitting (2.1 nm in diameter) and distinctive red-emitting (3.4 nm) CdTe QDs (see Supporting Information for nanocrystal optical characteristics). Real time confocal imaging

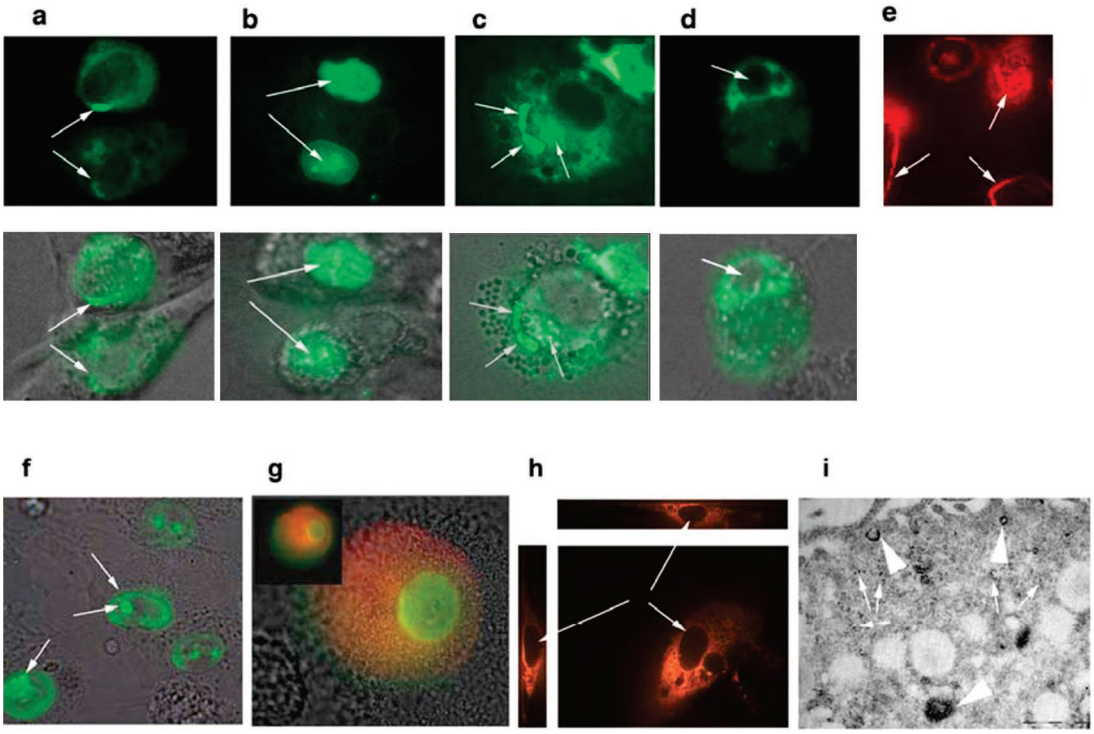

Figure 2. Green (2.1 nm) CdTe QDs are actively transported to the nucleus in macrophages. (a) Green CdTe QDs exhibit an early compact accumulation around the perinuclear membrane. Within 10 min, green CdTe QDs are sited perinuclearly (arrows). (b) Green CdTe QDs localize to the nucleus and the nucleolus (arrows). Later stage entry (30 min) is characterized by very intense green fluorescence in the nucleolus. (c) Nocodazole treatment blocks green CdTe QD accumulation in the nucleus. Macrophages were treated with nocodazole and incubated with green CdTe QDs for 40 min. Image shows diffuse cytoplasmic location and unidentified tubular structures (arrows). (d) Thapsigargin inhibits green CdTe QDs nuclear localization. 40 min time point from the beginning of cell exposure to QDs. "Empty" nucleus is denoted by arrow. (e) CdSe/ZnS 605 nm Qdot nanoparticles do not exhibit nuclear localization and are present at the membrane on the cell surface (arrows). Images were recorded at 30 min after addition of QDs to the cells. The central row of four images shows, at the same time, bright field images corresponding to the cells in panels a−d. QDs per se do not have any significant impact on the cell attachment, spreading, or integrity, reflecting their overall "healthy" condition (panels a and b). However, both nocodazole and thapsigargin do have negative effects on the cell attachment and spreading (panels c and d). These effects are unavoidable in the case of adherent cell lines, and reflect inhibitory effects of nocodazole on the microtubules (involved in cell adhesion) and adverse action of thapsigargin on Ca^{2+}-dependent intracellular signaling. (f) Green CdTe QDs injected directly into the nucleus retain their nuclear and nucleolar location after a 45 min observation period (arrows). (g) Mixture of red and green QDs injected into the cytoplasm separates into two distinctive cytosolic and nuclear compartments within 60 min of observation. Inset, same cell 15 min post-microinjection. (h) CdSe/ZnS QDs (3.8 nm) do not display any significant nuclear localization even after direct microinjection (arrows). (i) TEM image of red-emitting CdTe QDs uptaken by macrophages. QDs are present in the cytoplasm both as small isolated groups (arrows) and larger coated vesicles (arrowheads). The experiments were carried out in human monocyte-derived macrophages.

revealed rapid (within 30 min) and specific nuclear accumulation of the green QDs in the phagocytic cells (panels c and d of Figure 1) while the red QDs (Figure 1b) displayed a cytoplasmic compartmentalization (see also Figure 1(Supp) in Supporting Information). Early green CdTe QD uptake in THP-1 cells (10 min) shows a distinct perinuclear location (Figure 1a). Simultaneous addition of red and green CdTe QDs resulted in a specific size-selective nuclear localization of green QDs while the red QDs were retained in the cytoplasm (Figure 1c). Quantitative assessment of the intracellular fluorescence levels in individual cells revealed a rapid inverse shift in the prevalence of cytosolic versus nuclear localization of green CdTe QDs already after a brief 10 min incubation (Figure 1d,e). Very fast quantitative dynamics of QDs nuclear internationalization by THP-1 cells (Figure 1f) provides an immediate hypothesis of cell active transport mechanism implication in the QDs nuclear delivery in this cell line. This rapid accumulation was not associated with adverse cell viability as assessed by nuclear shape and fragmentation. No detectable accumulation of CdTe QDs in either of the other tested cells lines (HUVEC, AGS, or HCT-116) was observed over 2-h incubation periods using multiple time points on more than 300−400 cells by high content analysis technique, thereby reliably representing overall population responses. Importantly, overall negative nuclear/cytosolic fluorescence difference values registered in these cell types (and especially pronounced in HUVEC cells, Figure 1f) reflected exclusively nanoparticle accumulation over the cell membrane and did not represent any significant cytoplasmic uptake, as confirmed in subsequent Z-stack analysis of individual cells by confocal microscopy. We further addressed in detail the factors which may contribute to the uptake, intracellular transport, and selective nuclear accumulation of the smaller green CdTe QDs in macrophages.

Targeting of QDs Involves Active Cytoplasmic Transport Mechanisms. Figure 2a demonstrates the compact early accumulation of the green CdTe QDs around the perinuclear

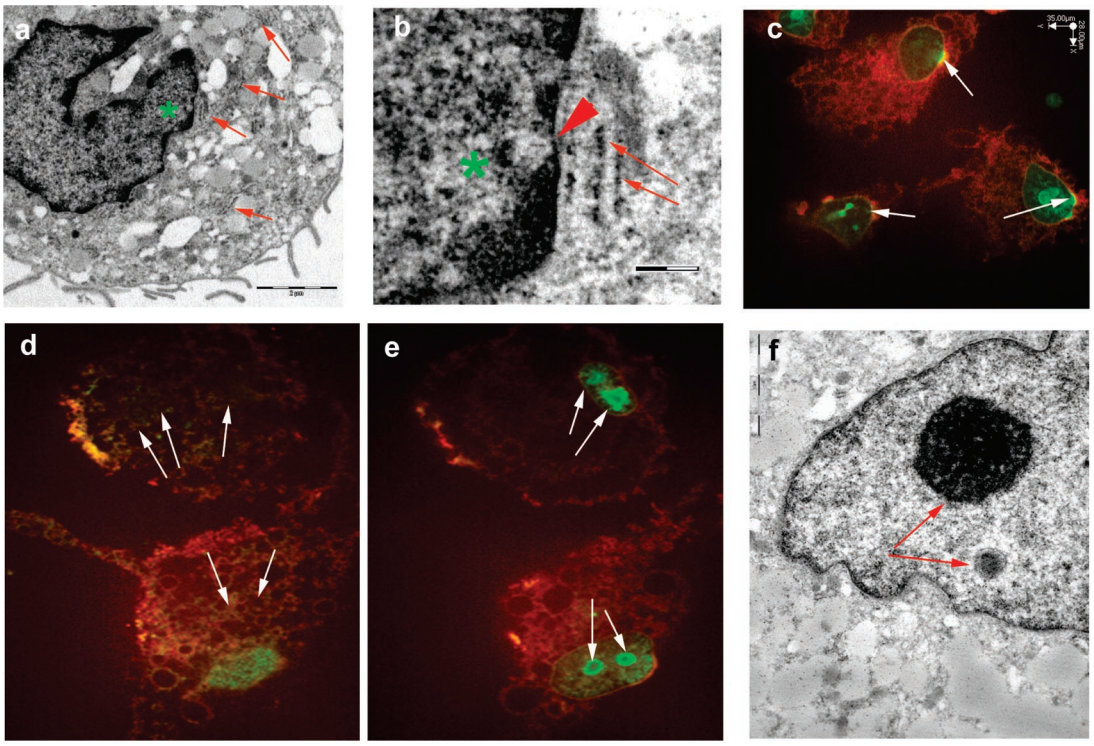

Figure 3. Size selective intracellular compartmentalization of green (2.1 nm) CdTe QDs in human macrophages. (a) TEM image illustrating QD location in the rough endoplasmic reticulum. Arrows points to the ribosome-rich ER membranes in the cytoplasm. Asterisk denotes the area magnified in (b). (b) TEM microphotograph showing QD concentration in the perinuclear ER (arrows). Arrowhead indicates the location of the nuclear pore. (c) Confocal optical section at the level of the ER demonstrating green and red CdTe QD location in macrophages. Green QDs are localized to the nucleus while red QDs display a diffuse cytoplasmic fluorescence. Both types of QDs colocalize at the perinuclear ER (yellow/orange color) indicated by arrows. (d, e) Two confocal optical planes showing QDs associated with cytoiplasmic ER, seen as weak green granular cytosolic staining indicated by arrows in (d) and nuleolar localization of green-emitting QDs, arrows in (e). (f) TEM image of macrophage nucleoli richly highlighted by accumulated QDs (arrows). The experiments were carried out in human monocyte-derived macrophages. Images correspond to 30 min time points following the initial contact of cells with QDs.

membrane prior to their accumulation within the nuclei and nucleoli (Figure 2b). Given the rapid direct movement of the green CdTe QDs (within 30 min) to their preferred nuclear position (Figure 1f), we examined the sensitivity of this response to treatment with an anti-microtubule agent nocodazole or with the anti-F-actin agent cytochalasin-D. Treatment with nocodazole resulted in suppression of nuclear localization and the retention of the green CdTe QDs within distinct cisternae-like endosome-like vesicles with a weak cytosolic component (Figure 2c) whereas the cytochalasin-D does not affect the QDs nuclear localization pattern. These data and the fact that at the early stage the majority of QDs are accumulated around the perinuclear region (Figures 1a and 2a) presume that the QDs are originally trapped in endocytic vesicles and these are subsequently transported by molecular motors along microtubule tracks to the perinuclear area. It is known that dynein is a microtubule minus-end-directed motor, which transports organelles cargos from the cell periphery to the perinuclear region, while kinesin moves in the opposite direction.[16,17] Although there are kinesin variants moving certain organelles toward the microtubule minus-end, endosomes have been shown to undergo active transport mediated by dynein in the direction of endoplasmic reticulum (ER).[9,16,17] Importantly, at some point during this process, QDs should be able to suspend the microtubule-dependent endosomes translocation escaping the endosomes and associate with the nuclear envelope (Figure 2a).

TEM in combination with confocal microscopy was used to confirm the QD endosome intracellular initial localization and to verify further intracellular location of green CdTe QD (Figure 2i, Figure 3, Figure 2(Supp), Figure 3(Supp)). After entering the cell, QDs are seen as electron-dense material in the perimembrane vesicles (Figure 2i) and cytoplasmic QDs-enriched "cisterns" reflecting endosome tubulation (Figure 2(Supp)). The dense packing of the QDs is reduced in the proximity of the nucleus (Figure 1(Supp)). TEM experiments also demonstrated that the QDs containing vesicular and tubulated endosomes are aligned with the surrounding microtubule filaments (Figure 3(Supp)) whereas the occurrence of organized endocytic structures is reduced in the proximity of the nucleus (Figure 1(Supp) and Figure 3(Supp)).

After 10 min of incubation, green QDs were found to colocalize with ribosome-rich ER structures throughout the cytoplasm (Figure 3a) and laterally at the nucleus (Figure 3b). High-resolution live confocal imaging of cells dual labeled with green and red QDs focused at the level of the ER uncovered that the red particles were retained in the cytosol and also colocalized with the green QDs at characteristic "bud"-like structures corresponding to the perinuclear

ER (Figure 3c). This observation of free QDs in the cytoplasm is an important result, suggesting that QDs can escape cytoplasmic vacuoles or elude sequestration (see below), which might allow interactions with cellular organelles or access to the nucleus. However, only the very small green QDs were able to penetrate further into the nucleus displaying here confined areas of compact concentration highlighting the nucleoli (Figure 3c and Movie 2 (Supporting Information)).

The nucleus protects its pool of RNA and ribosomes within the nucleolus. This power house within the nucleus assembles ribosomal subunits that must make their way through the NPCs to the rough ER to aid protein synthesis in the cytosol. Additional to the nucleolus, green QDs displayed compact perinuclear localization typical of the juxtanuclear portion of the rough ER.[15] This raises the intriguing possibility that very small green QDs may exploit similar or identical intracellular transport routes that are naturally operating between the nucleolus and the ribosome-rich perinuclear ER.

Thioglycolic Acid-Capped CdTe QDs Escape Endosomes. The ability of negatively charged CdTe QDs to escape the endosomes and to accumulate in proximity to NPCs represents a fascinating and somewhat controversial phenomenon. Jaiswal et al.[7] demonstrated that the negatively charged CdSe/ZnS QDs capped with dihydrolipoic acid are easily endocytosed by mammalian HeLa cells or *Dictyostelium discoideum* (AX2) cells, but the QDs were always present in a large number of endosomes distributed in a juxtanuclear region. In our case, the CdTe QDs capped with thioglycolic acid do not rest in endosomes (and do not end in lysosomes) but release in the cytoplasm and associate with the nuclear envelope.

We speculate that the CdTe QDs are changing their surface charge, within the acidic endosomes, from the strongly negative (at higher pH) to practically neutral due to the reprotonation at lower pH of their surface acidic function (thioglycolic acid) in exactly the same manner as it happens for the well-known lysosomotropic agents used to escape the endosomes in the course of intracellular drug delivery.[18] Cationic lipids or polyethylenimine[19] or poly(DL-lactide-*co*-glycolide) polymers,[20,21] for example, cause the swelling and rupture of the lysosomes by sequestering protons and their counterions due to the "proton sponge effect" and create an osmotic imbalance similar to that created by the other lysosomotropic compounds.[18] These proton sponges are effective at virtually any pH for polyethylenimine and cationic lipids and at acidic pH for poly(DL-lactide-*co*-glycolide) (PLGA) nanospheres and polymers. All these proton sponges (even at the absence of the charge reversal) are able to strongly protonate leading to an increase of intra-endosomal pH and a charge gradient provoking a water influx and endosomal swelling and disintegration.[18]

We have found very similar properties of CdTe QDs and lysosomotropic agent PLGA operating as a "proton sponge" at acidic pHs and highlighted a very similar behavior of CdTe QDs and PLGA within the cells. The lysosomotropic properties of PLGA are determined by its capacity to strongly protonate at acidic pHs characteristic for the endosomes.[18,20,21] PLGA is strongly negatively charged at basic and neutral pHs and coagulate around the pH which coincides with the dissociation constant of the carboxyl group (around pH4.0) due to the decrease in the zeta potential below a certain critical value needed for electrostatic solubilization.[21] Hence, the zeta potential measured at pH values where coagulation occurred does not represent the zeta potential of the nanospheres but the potential of the aggregates formed. Figure 4(Supp) shows that the CdTe QDs capped with thioglycolic acid are strongly negative at neutral and slightly basic pHs (nearly −50 mV), but at lower pH strongly protonate, (reversibly) aggregate at pH 4, and become practically neutral at the lower pH values. Moreover both compounds, QDs and PLGA, show practically identical pH-dependence of their zeta potentials when compared in identical conditions of measurement (Figure 4(Supp)). These similarities are not surprising taking into account that the surface charge properties of the both compounds are determined by the same functionality—carboxyl group of thioglycolic acid. The zeta potential−pH profiles shown in Figure 4(Supp) exhibit a plateau region at neutral and high pH, while at low pH values the shapes of the curves do change. It is interesting to note the presence of an inflection point in the zeta potential−pH profiles which may be used as an indication of the nature of the surface groups and their influence on the electrokinetic properties of colloid particles. For instance, an inflection point at a pH value about pH 6 for the QDs and PLGA nanospheres coincides with the presence of carboxyl groups.[21]

Reversible aggregation of CdTe QDs at pH values around 4 was previously described by us[22] and attributed to the transfer of protons from the bulk liquid to the QDs thioglycolic acid surface functionalities and carboxyl group protonation[23] but the significance of this effect in the escape of QDs from the endo-lysosomal compartment was not elucidated. This QD surface protonation could explain the differences in QD behavior in the different endocytic vesicles, very similar to those described for PLGA lysosomal escapes.[20]

What is even more important, the CdTe QDs demonstrate intra-endosomal behavior very similar to such for PLGA. The TEM photograph (Figure 1b(Supp)) shows that within the endosomes QDs are indeed presented in the form of dense clusters or aggregates. These data support our hypothesis that surface protonation of CdTe QDs in the endo-lysosomal compartment, followed by their reversible and pH-dependent aggregation, is responsible for their escape into the cytoplasm. The secondary endosomes and lysosomes are predominantly acidic, with pH values ranging around 4.[18] In this pH, QDs would have a net neutral potential and hence would interact with the negatively charged membrane, leading to their escape into cytoplasmic compartment. Lysosomotropic agents are known to cause the destabilization of endo-lysosomes because of the change in the pH of the endo-lysosomal vesicles, leading to the escape of their contents.[24]

After escape from the low-pH endosomes, QDs deprotonate and disaggregate at neutral and slightly basic pH becoming again strongly negatively charged.

QD Nuclear Transport. Following the escape from the endosomes, already within 10 min of incubation, the QDs

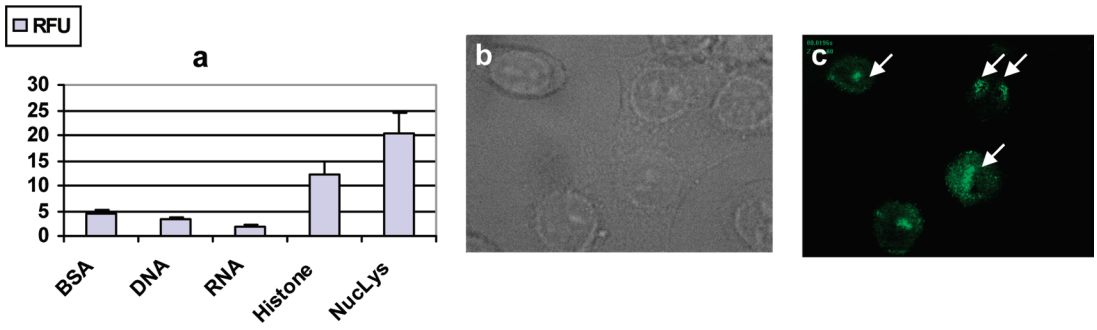

Figure 4. Histone targeting of CdTe QDs. (a) Dot blot analysis of CdTe QD binding to BSA, DNA, RNA, purified histones, and nuclear extract. Equal amounts of QDs were applied on the nitrocellulose membranes with prebound nucleic acids and proteins as indicated below the columns. *Y* axis shows the relative fluorescence units detected above each spot after washout of unbound QDs. (b, c) Transmitted light and fluorescent images, respectively, of THP-1 phagocytic cells immunostained for histones. Arrows indicate nucleolar histone accumulation sites.

showed compact perinuclear location (Figure 2a) near the NPCs (Figure 3a,b). In the next 20 min, the green QDs are localized to the nucleus and the nucleolus (Figure 2b). The nucleus is separated from the cytoplasm by a double membrane of nuclear envelope which is contiguous with the ER membrane.[15] Their cisternae are major intracellular calcium stores. Embedded in both nuclear membranes are large macromolecular structures, the NPCs, controlling nuclear transport in both directions. Small diffusional channels with a diameter of 5−9 nm are situated in the scaffolding NPCs framework and allow passive diffusion of molecules smaller than 25 kDa.[15] Depletion of calcium from the nuclear envelope by the calcium ATPase inhibitor thapsigargin blocks passive diffusion and signal-mediated transport most likely due to a steric block of the central and peripheral NPC transport channels.[25]

In our work, treatment of the cells with a thapsigargin prior to QD exposure demonstrated that the thapsigargin-treated macrophages failed to deliver the green CdTe QDs to the nucleus (Figure 2d). Importantly, thapsigargin cell treatment does not inhibit QDs targeting to the NPCs. Given the size specificity and active transport routes employed by the green CdTe QDs, we analyzed the subcellular distribution of substantially larger commercially available CdSe/ZnS Qdot nanoparticles[26] emitting in the red at 605 nm, in macrophages and polymorphonuclear leukocytes. Figure 2e displays comparable incubation of macrophages with 605 nm Qdot at the particle concentration (1 μM) equivalent to the previous experiments. Despite the very bright and stable fluorescence signal detected throughout the extended observation period (over 4 h), no specific localization pattern was observed in either cell type.

Impact of Bypassing the Membrane-Associated Phagocytic Mechanisms. We next evaluated the potential impact of bypassing the membrane-associated phagocytic mechanisms on the subcellular localization of QDs. Direct intranuclear microinjection delivery of green CdTe QDs did not affect their confinement within the nuclear envelope even after a long 45 min observation period (Figure 2f). At the same time, the mixture of green- and red-emitting QDs injected into the cytoplasm separated into two respective nuclear and cytoplasmic compartments within 1 h after the procedure (Figure 2g). However, the speed of the intranuclear accumulation of green QDs was in this case significantly slower compared to the above-described spontaneous transmembrane delivery route (within minutes), suggesting the contribution of active transport mechanisms operating at the level of the endosome vesicles.

Intracellular Transport of QDs of Different Chemical Origin. It was essential to find out if the other types of ultrafine semiconductor QDs behave similar to CdTe QDs in their ability to penetrate the cells and the nucleus. As indicated above, commercially available core−shell QDs are too large in comparison with our CdTe QDs, because they are synthesized in organics and have to be coated by extra shells to render them water soluble. Among these coating methods, the only one which allows keeping the size of water-transferred particles small enough is the treatment with DL-cysteine.[5] But even this method does not allow for obtaining QDs of 2−2.5 nm diameter, comparable in size with our green-emitting CdTe QDs. We have therefore taken the smallest available size of a core−shell CdSe/ZnS QD system synthesized in organics as described[27] and transferred to water by treatment with DL-Cys.[5] These QDs, with a size of 3.8 nm, did not enter the nucleus even following their intracytoplasmic injection (Figure 2h) thereby illustrating the unique properties of ultrafine CdTe QDs in this regard.

Histone Targeting of CdTe Quantum Dots. The conspicuous nucleolar localization of CdTe QDs has led us to investigate potential intracellular QD targets in more detail, since the accumulation of QDs possessing the ex synthesis net negative surface charge at a first glance contradicts to the abundant expression of similarly negatively charged nucleic acids DNA or RNA in the nuclear compartments. We have analyzed QDs binding to a panel containing nuclear lysate and major nuclear constituents by a dot blot technique (Figure 4a).

CdTe QDs demonstrated a strong affinity to nuclear lysates and displayed a significantly enhanced binding to purified histone protein, compared to BSA control, RNA, and DNA, as detected by dot blot fluorescent signal. Immunohistochemical staining using histone antibodies (Figure 4b,c) clearly confirmed a predominantly compact nucleoli localization of histones in THP-1 cells, in addition to diffuse nuclear

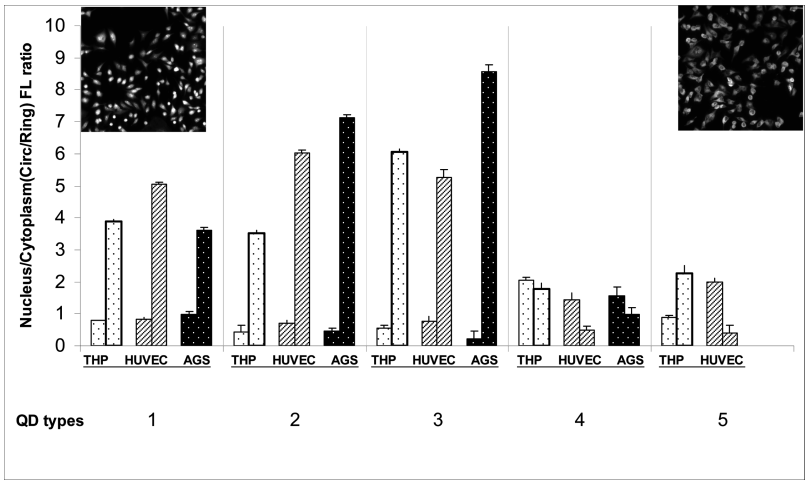

Figure 5. Cell fixation and permeabilization prior to CdTe and CdSe/ZnS QD exposure attenuate intracellular nanoparticle distribution selectivity. Nucleo/cytoplasmic fluorescence intensity ratios in THP-1 cells (dotted columns, THP), HUVEC cells (hatched columns, HUVEC), and AGS cell line (black dotted columns, AGS) in thioglycolic acid (TGA)-stabilized CdTe QDs of 2.1, 2.8, 3.0, and 3.5 nm diameter, respectively (sets 1−4) or DL-cysteine-stabilized 3.8 nm CdSe Zn/S core/shell QDs (set 5). QDs incubated with cells for 30 min. Left columns in each pair reflect the data from fixed cells. Right columns in each set represent data from cells fixed and additionally permeabilized prior to QDs exposure. Insets provide representative screenshots from the microscopic fields of the cells with predominantly nuclear (left) and cytoplasmically accumulated QDs (right). Data on AGS cells in set 5 are not available. Columns reflect mean values and standard errors obtained from at least 500 cells detected in random microscopic fields.

and dotted nuclear envelope associated staining patterns. These distribution patterns were identical to those displayed by QDs in human phagocytes (Figure 3d−f). If the strong electrostatic attraction of CdTe QDs to positively charged histone-enriched compartments in fact represents a leading mechanism for nuclear and nucleoli targeting of these nanoparticles in macrophages, it theoretically should hold true for the other cell types even in the absence of active phagocytic processes, provided that the cell and nuclear membranes possess sufficient permeability. We focused on this hypothesis in further detail by implementing the models of fixed and fixed/permeabilized cells.

QD Distribution within the Fixed and Fixed/Permeabilized Cells. A panel of phagocytic, vascular endothelial, and gastric epithelial cells exposed to green- and red-emitting QDs of different nature was analyzed by using the Cellomics Kineticscan high content screening workstation. As seen from Figure 5, cell fixation and permeabilization prior to QD exposure attenuated intracellular nanoparticle distribution selectivity. CdTe QDs with size of up to 3.0 nm were not present in the nuclei of fixed intact cells, independent of the particular cell type. Membrane permeabilization inverted the nucleo/cytosolic distribution ratios in favor of cell nuclei to a dramatic extent (Figure 5, sets 1−3) typically also brightly decorating the nucleoli. CdTe QDs of 3.5 nm diameter (set 4) and above (not included in the graph) along with 3.8 nm CdSe/ZnS nanoparticles (set 5) were not capable of pronounced nuclear entry. These findings additionally confirm that contrary to the size-cut of passive diffusion mechanisms operating in fixed and fixed/permeabilized cells (Figure 5), active transport processes are functioning at the level of nuclear gate entry in intact phagocytic cells (Figures 1−3). In the case of paralyzed nuclear transport machinery (fixed cells), a size-specific cutoff band at approximately 3.8−4 nm still holds true, despite the forced permeabilization of the cell membrane (Figure 5). Substitution of TGA with mercaptopropionic acid (MPA) as a stabilizing agent did not significantly alter the earlier observed green- and red-specific QDs compartmentalization pattern; however, it detectably enhanced the fluorescent signal from nucleoli (data not quantified).

Discussion. The ability of CdTe and CdSe/ZnS QDs to exploit cell's active transport machinery delivering them to perinuclear location in ER and ability of ultrafine CdTe QDs to be delivered and accumulate in the nuclei and nucleoli represent a fascinating phenomenon with possible far-reaching consequences. Although the phagocytic cells have developed a specific set of particle-engulfing mechanisms which significantly differ from clathrin-controlled receptor-mediated endocytosis typical of most other cell types, these pathways are mostly specific for uptake of quite big (>0.5 μm) particles.[28] Negatively charged CdTe and CdSe/ZnS QDs used in our studies penetrate human macrophage cells through endocytosis and enter the cytosol being included in the endosome-like vesicles (similar to those described by Jaiswal et al.[7] for CdSe/ZnS QDs capped with dihydrolipoic acid) and are transported to the perinuclear ER membranes. The smallest CdTe QDs were able to enter, on a minutes time scale, the nuclear and nucleoli of live human macrophages where they associate with the positively charged histone proteins.

Regarding the specificity of the QDs uptake by phagocytes, we feel it appropriate to refer to the previously published observations. Unlike many other cell types, monocyte-derived macrophages and THP-1 cells are able to express scavenger receptors in high abundance upon cell activation.[29,30] These scavenger receptors recognize and mediate the uptake of the negatively charged compounds and modified low-density lipoproteins. On the other hand, it has been recently reported that nanoparticle uptake by phagocytes is stimulated in favor

of carboxy-dextran-coated iron oxide nanoparticles compared to those coated with nonionic dextrans.[31] In addition, there is factual evidence that in the phagocytic cells, the presence of the negative charge on the surface of ingested material can facilitate its efficient entry into the cell.[32,33] In the poorly differentiated HeLa type cells known to be capable of active endocytosis, it has been shown that Salmonella mutants with a propensity to hydrophobic interaction and negative surface charge were attached and internalized to a greater extent than bacteria lacking such surface properties.[34] Of note, our TEM data show that the endocytotic process in the case of negatively charged CdTe quantum dots is accompanied not only by the formation of typical spherical vesicles but also frequently by the formation of extended membrane invaginations appearing as elongated "cistern-shaped" structures reflecting the endosome tubulation process. This process has been very recently reported to be induced by fatty acids-rich lipopolysaccharide in dendritic cells capturing exogenous antigenic material.[35]

To enter the nucleus a particle must be chaperoned by a transport factor through the nuclear pore complex or it must be small enough to pass through by diffusion.[17] As an example, the membrane proteins with extralumenal domains that are $<\sim$25 kDa can efficiently diffuse throughout all the ER subdomains.[17] According to the microelectrode data obtained in intact cell nuclei of various species,[36] cell-type-specific differences in electrical dimensions of nuclear pores could prove to be critical for size-selective QD penetration into the nucleoplasm. These dimensions have been estimated as varying between 1.3 and 3.6 nm for several cell types, including epithelia of salivary glands and kidneys, pronucleus and oocytes and reaching 5.2 nm only in liver cells, among all other types presented.[36] Although we currently have no data on comparative analysis of the effective electric dimension of nuclear pores in phagocytic cells with other cell types investigated in our study, the possibility of existing differences falling within the range of variation of green to red QDs diameters and reflecting their nuclear entry capability hence stands as entirely possible. In addition, QDs due to their size and physical characteristics could be considered rather as more closely related to rigid oligo-molecular and ion structures rather than to highly flexible peptides and proteins capable of significant deformability. From this perspective, even significantly larger size polypeptide molecules and immunoglobulins exceeding 15−20 nm in diameter might display a seemingly controversial ability to squeeze through the much smaller biological pore-decorated barriers. In contrast, under similar circumstances even the smallest QD aggregates consisted of four to five nanocrystals, practically undetectable in biological systems, can be completely cut off by the restricting pore size. This opens up an opportunity to exploit such size-specific separation mechanism for generation of new classes of highly selective drug delivery systems.

Of note, among the limited available data confirming the size-specific nuclear distribution specificity of green-emitting versus red-emitting QDs, the results of the studies by Lovrić et al. performed in N9 murine microglial cells exposed to MPA-stabilized CdTe QDs[12] strongly support our findings. Furthermore, at the cell membrane level, larger particles (including those over 5 nm in diameter) are more likely to be utilizing intracellular uptake routes involving phagosomes and other mechanisms rendering them coated in membrane material thereby significantly increasing the overall size of the transported structure precluding its efficient nuclear entry.

Our study provides the first direct evidence of QD intracellular active transport mediated by interaction with histone proteins and suggests a mechanism of QD targeting to histone-rich intracellular compartments, which in most mammalian cells correspond to the nuclei, nucleoli, and ribosome-associated rough ER. From this perspective, it is important to highlight that histones play an important regulatory role in the normal cell cycle and tumor growth due to their ability to undergo dynamic reversible acetylation. In line with this fact, as can be seen from the Figure 1c, nearly 40% of the cells do not have green QDs in their nucleus. Our unpublished observations indicate that the level of QD association with nucleoli varies also within the cell populations. These variations possibly reflect relevant stages of cell cycle and hence the degree of histone acetylation involved in cell cycle progression,[37] QDs might potentially have a differential "tropism" for these proteins at some stages of cell cycle. We are currently exploring this hypothesis in detail in a separate study. This is an intriguing phenomenon with potentially far-reaching consequences raising an intriguing opportunity to directly monitor and manipulate cell cycle progression at the nanoscale level. Nanoparticle uptake by different cell types can also potentially reflect variations in their functional condition, cell cycle, and cell activation status.

Conclusion. Development of appropriate drug delivery systems based on the results of our study could allow cytotoxic and contrasting agents to selectively locate in the nuclear compartment with the potential for therapeutic or diagnostic imaging use. Our findings are also important in the context that even nonfunctionalized nanoparticles would be expected to be present to the human body at epithelial surfaces in skin, bronchial lining, and mucosal surfaces. The ability of cells derived from the monocyte macrophage lineage to internalize nanoparticles suggests the possibility that they would be selectively uptaken by cells such as the alveolar macrophage upon environmental exposure. Size- and charge-selective nuclear delivery of QDs in human cells offers an outstanding potential for bioimaging and therapeutics. On the other hand, even in the absence of cytotoxic effects of QDs observed in this study over the 72 h incubation period, QD specific intracellular accumulation may produce unknown delayed effects long term. Rapid nuclear localization of QDs demonstrated in our study clearly emphasizes the importance of strict environmental control of nanoparticles.

Methods. Synthesis of Quantum Dots. CdTe QDs of different sizes in the range 2−6 nm were synthesized directly in water according to the previously published procedure by employing thioglycolic acid as a capping agent.[38] Sizes of CdTe NCs referred to in this paper have been determined

from a sizing curve of ref 39 and were always 2.1 nm when we are speaking about "green" QDs and 3.4 nm when we are speaking about "red QDs". CdTe QD coating in all experiments presented in a paper was always thioglycolic acid (TGA) if no other coating is mentioned. The QDs surface charge depends on the pH and buffer or the microenvironment. pH-dependent variation of QDs zeta potential is shown in Figure 4(Supp). The QDs were washed out from the excess of nonreacted reagents by precipitation with 2-propanol and redissolution in water resulting in solutions of 10^{-4} M particle concentration. These solutions were stable for more than a year allowing multiple comparative compartmentalization studies. Water-soluble CdSe/ZnS 605 nm emitting QDots were purchased from Invitrogen and used as received.[26] We have also synthesized a green-emitting CdSe/ZnS as described in ref 27 and solubilized them with a DL-cysteine as described in ref 5. These CdSe/ZnS QDs were found to be 3.8 nm in diameter.

High Content Analysis. High content quantitative analysis of QDs interactions with live and fixed cells was performed on the Cellomics Kineticscan workstation. Cells were plated out approximately at 9000−15000 per well, depending on the cell type in 96-well plates (Packard, PackardView 96 Black) in 175 μL culture medium. Cell fixation was performed with 2.5% glutaraldehyde, followed (in some experiments) with permeabilization by 0.1% Triton X-100 at ambient temperature for 30 min. Cells were incubated with QDs samples as indicated in the Figure 5 legend for 30 min in complete culture medium (containing serum), followed by washing of the unbound particles by repeated gentle pipetting. The optimized image acquisition algorithm was based on the Compartmental Analysis (Cellomics) bioapplication utilizing a built-in "CircRingAvgIntenRatio" parameter as a major criterium for quantification of nuclear to cytosolic fluorescence intensity ratio in QD-containing cells. With the HCS instrumentation, large variances between the intensities of QDs were observed, rendering it necessary to reset image acquisition parameters (such as exposure times). This made comparisons of compartmental localization of QDs based on pixel intensity alone difficult. The ratiometric parameter described above allows direct comparisons to be made between different QDs with distinctive light emission characteristics. It allows accurate quantification of the spatial distribution of QDs in the cells in terms of relative pixel intensity independent of absolute value for intensity of emitted light; 505 and 550 nm bandpass channels were used for green and red fluorescent QDs, respectively, and the blue (460 nm) channel for the detection of Hoechst nuclear counterstain. All readouts included the experimental conditions duplicated or triplicated in separate wells.

Cells and Cell Lines. Human THP-1 monocyte cell line and transformed epithelial cell lines HCT-116 and AGS were obtained from the European Collection of Animal Cell Cultures (ECACC, Salisbury, U.K.). Vascular endothelial HUVEC cells were isolated from human umbilical cord material and used between passages 3−8. Human monocyte-derived macrophages were prepared using the easy step positive selection method (Stem Cell Technologies). Cells were grown in RPMI 1640 medium supplemented with 10% heat-inactivated foetal bovine serum (FBS), 2 mM l-glutamine/L, 100 μg of penicillin/mL and 100 mg of streptomycin/mL, and incubated at 37 °C in 5% CO_2 in all experiments. To induce monocyte to macrophage differentiation, THP-1 cells were cultured in the presence of 100 ng/mL phorbal myristate acetate (PMA) for 72 h. Cells were then washed three times with Hank's balanced salt solution before use. Human macrophages and differentiated THP-1 were treated with Nocodazole (20 μM) and Thapsigargin (100 mM) for 30 min prior to addition of QDs. QDs were then added at 1:100 v/v dilution (for the times indicated in the text and/or figure legends) in complete (serum-containing) culture medium.

Imaging and Microinjection. Live cell imaging was performed in Lab-Tek chambered coverglass slides (Nunc) using a 100× oil immersion objective lens. Microinjection was carried on an inverted Nikon TE300 microscope with Narishige hydraulic micromanipulation and microinjection equipment and utilizing ex tempore fabricated glass capillary microneedles with 0.1−0.15 μm i.d., backfilled with QD solutions in the culture medium. Images were acquired by fluorescence microscopy (Nikon Eclipse TE 300) and on the UltraView Live Cell Imager confocal microscopy workstation (Perkin-Elmer Life Sciences, Warrington, U.K.) with laser excitation wavelengths at 488 and 568 nm and emission filters at 525 and 600 nm for green and red fluorescence detection, respectively. Processing and three-dimensional (3-D) image analysis were performed using Ultra View LCI and Volocity-2 software (Improvision). In addition to experiments utilizing high content analysis equipment, quantitative evaluation of intracellular fluorescence levels was also performed on the still picture frames using the NIH Image software. Inverted gray scale density values were calculated from the manual outlines of cell areas corresponding to cytoplasmic and nuclear compartments.

Electron Microscopy. For transmission electron microscopy studies, cells in culture were fixed with 2.5% glutaraldehyde in 0.1 M Sorensen phosphate buffer pH 7.2 for 1 h at room temperature. After the cultures were washed in buffer, they were postfixed with 1% OsO4 in 0.1 M Sorensen phosphate buffer pH 7.2 for 1 h at room temperature. The samples were then dehydrated in ascending concentrations of ethanol and embedded, in situ, in Epon resin using standard methods. To ensure an adequate number of cells for analysis, the specimens were sectioned en faces at a thickness of 100 nm using a diamond knife. Sections were retrieved onto naked copper grids and stained with uranyl acetate and lead citrate (for visualization of subcellular structures in control and orientation samples) or kept unstained for the studies involving nanoparticles, to avoid any possible masking of the QD distribution patterns by heavy metal depositions. Both stained and unstained sections were examined in a Tecnai Twin (FEI) transmission electron microscope at an accelerating voltage of 120 kV and using an objective aperture of 10×. Digital images were acquired using a MegaView camera, and measurements were made using the associated AnalySis software package.

Acknowledgment. This work was supported by SFI under Grant Number 02/IN.1/I47. Part of the work was supported by the European Union Sixth Framework Programme Consortium NanoInteract. A.R. was supported by SFI Walton Award and by the Excellence Cluster "Nanosystems Initiative Munich" (NIM) of the DFG. I.N. and A.S. acknowledge financial support from NATO and INTAS Innovation Programs. A.S. is grateful to FEBS for providing a long-term fellowship and follow-up funds. I.N. acknowledges partial support from ANR-PNANO and ANR-RIB programs. We also acknowledge the support of Enterprise Ireland (Research Innovation Fund) under Grant Number IF/2002/656, Health Research Board of Ireland (Grant RP/2006/246), and thank Professor Dr. H. Weller and Professor Dr. A. Eychmüller for useful discussions.

Supporting Information Available: Movie I shows selective subcellular distribution of green- and red-emitting CdTe QDs in live human macrophages, demonstrating three-dimensional reconstruction of the confocal optical Z-stack showing green CdTe QDs in the nuclei and red QDs exclusively in the cytosolic compartment; Movie II demonstrates that the green CdTe QDs are accumulating in the nuclei and particularly in histone protein-enriched nucleoli of human macrophages, showing sequential confocal optical slices illustrating a complex nucleolar structure; Figure 1(Supp) dynamics of intracellular accumulation of green (2.1 nm) and red (3.4 nm) CdTe QDs in the macrophage-like THP-1 cell line and epithelial cells; Figure 2(Supp) endosomal uptake of the quantum dots; Figure 3(Supp) association of endocytic compartments containing QDs with microtubules; Figure 4(Supp) zeta potential of the thioglycolic acid-covered CdTe quantum dots as a function of pH; Figure 5(Supp) optical characteristics of QDs used in the study. This material is available free of charge via the Internet at http://pubs.acs.org.

References

(1) Alivisatos, P. *Nat. Biotechnol.* **2004**, *22*, 47.
(2) Smith, A. M.; Dave, S.; Nie, S.; True, L.; Gao, X. *Expert Rev. Mol. Diagn.* **2006**, *6*, 231.
(3) Smith, A. M.; Ruan, G.; Rhyner, M. N.; Nie, S. *Ann. Biomed. Eng.* **2006**, *34*, 3.
(4) Alivisatos, A. P.; Gu, W.; Larabell, C. *Annu. Rev. Biomed. Eng.* **2005, *7***, 55.
(5) Sukhanova, A.; et al. *Anal. Biochem.* **2004**, *324*, 60.
(6) Chen, F.; Gerion, D. *Nano Lett.* **2004**, *4*, 1827.
(7) Jaiswal, J. K.; Matoussi, H.; Mauro, J. M.; Simon, S. M. *Nat. Biotechnol.* **2003**, *21*, 47.
(8) Knight, V. B.; Serrano, E. E. *Proc. SPIE* **2006**, *6096*, 60960Y.
(9) Duan, H.; Nie, S. *J. Am. Chem. Soc.* **2007**, *129*, 3333.
(10) Ryman-Rasmussen, J. P.; Riviere, J. E.; Monteiro-Riviere, N. A. *J. Invest. Dermatol.* **2007**, *127*, 143.
(11) Shiohara, A.; Hoshino, A.; Hanaki, K.-I.; Suzuki, K.; Yamamoto, K. *Microbiol. Immunol.* **2004**, *48*, 669.
(12) Lovrić, J.; et al. *J. Mol. Med.* **2005**, *83*, 377.
(13) Lovrić, J.; et al. *Chem. Biol.* **2005**, *12*, 1227.
(14) Cho, S. J.; Maysinger, D.; Jain, M.; Roder, B.; Hackbarth, S.; Winnik, F. M. *Langmuir* **2007**, *23*, 1974.
(15) Cook, A.; Bono, F.; Jinek, M.; Conti, E. *Annu. Rev. Biochem.* **2007**, *76*, 647.
(16) Murray, S. *Nat. Rev. Mol. Cell Biol.* **2007**, *8*, 195.
(17) Lusk, C. P.; Blobel, G.; King, M. C. *Nat. Rev. Mol. Cell Biol.* **2007**, *8*, 414.
(18) Mukherjee, S.; Ghosh, R. N.; Maxfield, F. R. *Physiol. Rev.* **1997**, *77*, 759.
(19) Boussif, O.; Lezoualc'h, F.; Zanta, M. A.; Mergny, M. D.; Scherman, D.; Demeneix, B.; Behr, J. P. *Proc. Natl. Acad. Sci. U.S.A.* **1995**, *92*, 7297.
(20) Panyam, J.; Zhou, W. Z.; Prabha, S.; Sahoo, S. K.; Labhasetwar, V. *FASEB J.* **2002**, *16*, 1217.
(21) Stolnik, S.; Garnett, M. C.; Davies, M. C.; Illum, L.; Bousta, M.; Vert, M.; Davis, S. S. *Colloids Surf., A* **1995**, *97*, 235.
(22) Susha, A. S.; Javier, A. M.; Parak, W. J.; Rogach, A. L. *Colloids Surf., A* **2006**, *281*, 40.
(23) Gao, M.; Kirstein, S.; Mölhwald, H.; Rogach, A. L.; Kornowski, A.; Eychmüller, A.; Weller, H. *J. Phys. Chem. B* **1998**, *102*, 8360.
(24) Shitara, Y.; Kato, Y.; Sugiyama, Y. *J. Controlled Release* **1998**, *55*, 35.
(25) Perez-Terzic, C.; Pyle, J.; Jaconi, M.; Stehno-Bittel, L.; Clapham, D. E. *Science* **1996**, *273*, 1875.
(26) Information on size of commercially available Qdot samples of the Invitrogen Corporation: http://probes.invitrogen.com/products/qdot/.
(27) Baranov, A.; et al. *Phys. Rev. B* **2003**, *68*, 1653061.
(28) Aderem, A.; Underhill, D. M. *Annu. Rev. Immunol.* **1999**, *17*, 593.
(29) Vosper, H.; et al. *J. Biol. Chem.* **2001**, *276*, 44258.
(30) Iwashima, Y.; et al. *Biochem. Biophys. Res. Commun.* **2000**, *277*, 368.
(31) Metz, S.; et al. *Eur. Radiol.* **2006**, *16*, 598.
(32) Greenspan, P.; Ryu, B. H.; Mao, F.; Gutman, R. L. *Biochim. Biophys. Acta* **1995**, *1257*, 257.
(33) Magnusson, K. E.; Stendahl, O.; Stjernstrom, I.; Edebo, L. *Immunology* **1979**, *36*, 439.
(34) Kilhstrom, E. *Am. J. Clin. Nutr.* **1980**, *33*, 2491.
(35) Vyas, J. M.; Kim, Y. M.; Artavanis-Tsakonas, K.; Love, J. C.; Van der Veen, A. G.; Ploegh, H. L. *J. Immunol.* **2007**, *178*, 7199.
(36) Mazzanti, M.; Bustamante, J. O.; Oberleithner, H. *Physiol. Rev.* **2001**, *81*, 1.
(37) Jenuwein, T.; Allis, C. D. *Science* **2001**, *293*, 1074.
(38) Gaponik, N.; et al. *J. Phys. Chem. B* **2002**, *106*, 7177.
(39) Rogach, A. L.; Franzl, T.; Klar, T. A.; Feldmann, J.; Gaponik, N.; Lesnyak, V.; Shavel, A.; Eychmüller, A.; Rakovich, Y. P.; Donegan, J. F. *J. Phys. Chem. C* **2007**, *111*, 14628.

NL0719832